Simulation of Single Particle Displacement Damage in Silicon – Part I: Global Approach and Primary Interaction Simulation

Mélanie Raine, *Member, IEEE,* Antoine Jay, Nicolas Richard, *Member, IEEE,* Vincent Goiffon, *Member, IEEE,* Sylvain Girard, *Senior Member, IEEE,* Marc Gaillardin, *Member, IEEE,* Philippe Paillet, *Senior Member, IEEE*

Abstract— A comprehensive approach is developed for the simulation of Single Particle Displacement Damage in silicon, from the incident particle interaction in silicon, to the resulting electrical effect observed experimentally. The different steps of the global approach are described. The paper then focuses on the first step corresponding to Monte Carlo simulation of the primary interaction. The characteristics of the Primary Knock-On Atom (PKA) generated by neutron- or proton-silicon interactions for different energies are explored, analyzing in particular the PKA range in energies and species. This leads to the selection of 1 and 10 keV silicon atoms as good candidates to best represent the displacement cascades generated by all PKA. These PKA characteristics will be used as input in the following Molecular Dynamics simulation step, developed in a separate paper to simulate the displacement cascade generation and evolution. Monte Carlo simulations are also performed in a geometry representative of an image sensor, analyzing the distribution of non-ionizing deposited energy. The obtained distributions appear very similar for incident neutrons from 3 to 18 MeV and incident protons of 200 MeV, in agreement with similarities observed in experimentally measured dark current distributions in image sensors. The effect of geometric parameters on these distributions is finally explored.

Index Terms— Single-Particle Displacement Damage (SPDD), neutrons, dark current distribution, annealing, Active Pixel Sensor (APS), CMOS Image Sensor (CIS), Monte Carlo simulations, PKA, NIEL.

I. Introduction

Because of historical interest for space applications, Displacement Damage (DD) dose effects have been studied for a long time, with an extensive body of work on image sensors (Charge-Coupled Devices (CCD) at first and more recently Active Pixel Sensors (APS) or CMOS Image Sensors (CIS)), which dark current distributions directly reflect DD effects on minority carrier generation rate. With an increasing range of applications for image sensors – high energy physics, fusion, or even medical facilities – understanding these effects is more crucial than ever, in the hope that mitigating techniques can be deduced from their analysis.

In this perspective, the key issue is to link the macroscopic electrical effect observed experimentally (dark current in image sensors) to microscopic damage structures generated at the atomic level. One of the striking aspects of DD experimental data, on image sensors in particular, is the similarities observed in the response to irradiations with different particles on large energy ranges. Indeed, many studies have been dedicated to the modeling of dark current distributions, resulting in analytical models calculating either the average (e.g. [1-3]) or the distribution itself [4-8]. Among these, [3] and [8] succeed in proposing empirical models depending only on DD dose, whatever the nature of the incident particle (neutron, proton or heavy ion) or its energy (from fission neutrons to several hundreds of MeV protons). Likewise, the average dark current evolution exhibits similar annealing trends for all these particles and energies, from 100 ms to several days after irradiation [3], [9]. To our knowledge, only one recent study shows a different behavior for 200 and 700 keV neutrons [10], requiring an adjustment of the parameters of the model from [8]. With this exception for low energy neutrons, all these empirical observations seem to indicate that the induced electrically observable defects could have a similar nature, or at least that one kind of defect dominates the minority carrier generation rate, whatever the energy of the incident particle. In fact, the empirical results presented in [3] were modeled and interpreted later in [11] in terms of the production and dominance of defect clusters produced by particles with relatively high NIEL values. The present work thus aims at confirming this analysis and see if particular defect clusters are identified more often than others. Moreover, the generic empirical model presented in [3] is obtained from experimental data on many types of devices, including fabrication using n- and p-type material with various doping types and concentrations. This indicates that dopants have limited impact on the device response; this study thus ignores them in the following, focusing on the simulation of intrinsic silicon.

M. Raine, N. Richard, M. Gaillardin and P. Paillet are with CEA, DAM, DIF, F-91297 Arpajon, France (e-mail : melanie.raine@cea.fr).

A. Jay and V. Goiffon are with ISAE, Université de Toulouse, 10 av. E. Belin, F-31055 Toulouse, France.

S. Girard is with Univ-Lyon, Laboratoire H. Curien, UMR CNRS 5516, 18 rue du Pr. Benoît Lauras 42000, Saint-Etienne, France.

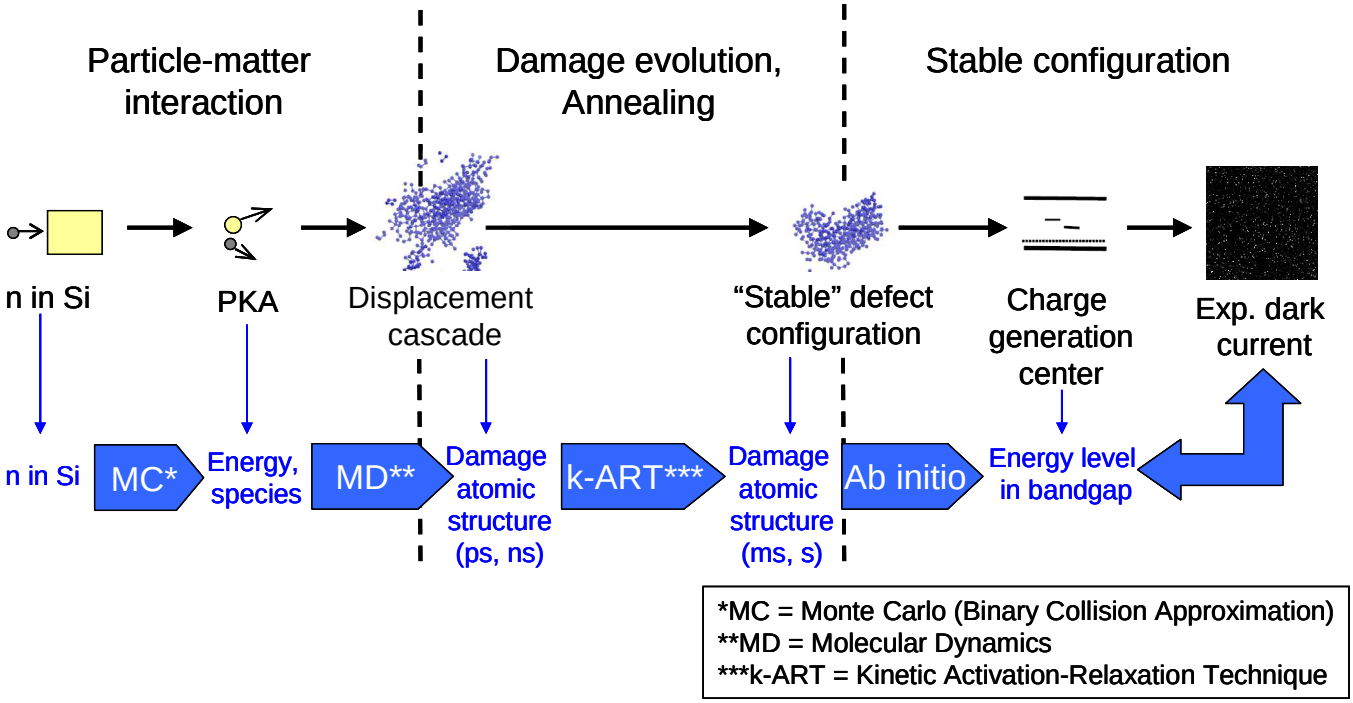

Figure 1: Schematic of the global simulation project

To identify atomic damage structures responsible for these similar DD effects, an ambitious multi-physics simulation project is started, aiming at combining different kinds of simulation, covering different timescales, to make the link between the atomic displacement at the lattice level, and the resulting electrical effect measured in image sensors. This project is envisioned as a long term effort, and extensive care will be given to the analysis of each step of the process. In this paper, we will first present the general methodology, and then focus only on the first simulation step, corresponding to the Monte Carlo (MC) simulation of interaction between the incident particle, either neutron or proton, and the target material, silicon here. The following simulation steps will be presented in details in dedicated papers, along with their respective advantages and limitations, in order to have sufficient space for analysis of each step and presentation of results.

The first goal of this paper is thus to identify the relevant output parameters than can be extracted from MC simulation, to be used as input in subsequent simulation step. The second goal is to see what knowledge can be drawn on DD mechanisms from MC simulation. Indeed, while MC simulation have been used to study DD [7, 12], most studies actually tried to develop a dark current prediction method, to reproduce experimentally observed dark current distributions or are based on high energy recoil cascade simulations only, as done with MARLOWE [13] for example in [14]. In this paper, a systematic simulation study will be performed focusing on the characteristics of neutron and proton interactions with Si and results will be analyzed in details, in an effort to find common features that could explain the similar experimental behavior observed in image sensors, for different kinds of particles on a large range of incident energies. The final aim is to understand why the different proposed empirical models work in so many different cases, but also to identify their potential limits of application, in cases that may not have been tested and observed yet (unusual particle species or energy, more integrated devices...).

II. Presentation of the Global Simulation Project

The global simulation project, inspired from the one proposed by Srour and Palko in [15], goes from the incident particle interaction in the target material to the resulting electrical effect observed experimentally (Figure 1). This figure first describes the succession of phenomena at stake, and then identifies the corresponding simulation technique chosen for each step of the process, the output of one step being the input of the next. Combining different techniques allows covering large time scales, from the fs for the interaction itself to long-term evolutions observed after seconds or minutes. In this approach, identifying the relevant output of each simulation step to be used as input in the next step is a crucial task. Indeed, because of simulation limitations, the complete simulation of all cases is not realistic. On the contrary, simulating only one particular case would not be representative of measured experimental data, which involve stochastic processes inherent to the particle-matter interactions. Several events are thus simulated at each step, to get a database of possible structures of damage, among which representative cases are selected when the number of simulations needs to be reduced from one step to the next. Depending on the type of simulation and on computational constraints, compromises may thus have to be found, relying on a good assessment of the representativeness of chosen

simulation cases.

The first step is a MC simulation of the interaction between an incident particle (neutron or proton in the following) and silicon, in the Binary Collision Approximation (BCA). While this type of code can follow the trajectory of all secondaries generated by n/p-Si interactions, the BCA is considered to break down below ~1 keV, also [16] indicates that for the particular case of silicon recoils in silicon, this limit could be lowered to less than 100 eV. This step is thus mainly used to identify the first generation secondaries, and the output is a list of these secondaries, called Primary Knock-On Atoms (PKA), identified by their species and energy. The first goal of this paper is to identify among these PKA the most statistically relevant ones to be studied in following steps. Some characteristics of the resulting displacement cascade will also be explored, such as the general spatial distribution of deposited energy and its partition between ionizing and non-ionizing events.

After selecting relevant PKA from MC results, the next step is a classical Molecular Dynamics (MD) simulation of the trajectory of selected PKA in silicon, with the detailed displacement cascade and the first steps of its evolution. MD methods indeed allow simulating the simultaneous motion of all atoms in the damaged region, taking into account the diffusion-limited kinetics and potential reorganization of the displaced atoms. This step is limited by the size of the system considered in the simulation and the characteristic accessible timescale, which prevent from studying the evolution beyond nanoseconds after the initial interaction. In our case, the output is a database of atomic structures of damage for different incident PKA (energy, direction), nanoseconds after the initial event.

To explore the evolution of this structure over longer periods of time (up to seconds and more) and reach time scales comparable with experimental data, a new technique called the kinetic Activation-Relaxation Technique (k-ART) [17] is then used. Starting from an initial atomic configuration, this method explores the energy landscape to find all possible configurations around the initial one, classifying them depending on their activation energy and occurrence probability. Monte Carlo methods are then used to make the system evolve, on much longer times compared to previous methods. Moreover, this method is off-lattice, i.e. atoms can be present on sites that do not correspond to crystalline positions of the lattice, allowing to treat amorphization phenomena, contrary to kinetic Monte Carlo methods for example. Similarly to MD, the output is a database of atomic structures of damage, but going up to seconds after the initial event. At this stage, an analysis of the obtained structures is performed to determine the most recurrent ones or find rules to classify the obtained clusters.

Finally, *ab initio* (or first principles) calculations are performed using the GW approximation to calculate the electronics properties of the selected atomic damage structure. The output is, for each selected atomic damage structure, the energy levels introduced in the bandgap. From here, it will be possible to directly compare the simulation results with experimental data on APS devices.

The originality of this comprehensive approach is to link these different types of simulations that are usually performed independently, to obtain realistic damage structures representative of what results from the initial neutron/proton-silicon interaction. The new tool k-ART will also allow reaching much longer simulated timescales than what is usually achieved, resulting in damage structures compatible with the timescale of experimental data. This paper focuses on the MC step and the choice of relevant output to be used in MD. The MD and k-ART simulation steps are presented in a second paper [18]. The final *ab-initio* step will be the subject of future papers.

III. Monte Carlo simulation details

This paper focuses on the first step of the global project, i.e. MC simulation in the BCA. These simulations are performed using the Geant4 toolkit version 10.1 [19, 20]. Two different kinds of simulation are performed: a first one to explore the general characteristics of neutron/proton-Si interactions and identify PKA of interest, and a second one to explore first results regarding general characteristics of the displacement cascade (range, non-ionizing energy deposit...). This last kind of simulation is performed both in an infinite geometry and in a geometry representative of an image sensor. Separating these different steps will allow distinguishing the features directly related to the neutron/proton-matter interactions and cascade characteristics from the ones related to the geometry of the device of interest.

For the first type of simulation, the developed test application is based on the Geant4 “Hadr04” example. The geometry is reduced to a single cube of silicon with a 1 m dimension, representing a quasi-infinite homogeneous material, i.e. all incident particles will interact in the material. The intent being to focus first on neutron/proton-matter interactions, only processes relevant to these particles are registered, corresponding to the neutronHP package for neutrons and taken from the QGSP_BIC processes for protons. Incident particles are emitted isotropically from a point source located at the center of the silicon box. All secondary particles are killed (i.e. not tracked) after production; only their primary characteristics (type and energy) are registered. Each incident particle interacts once and only once in the simulation.

In the second type of simulation, the PKA trajectory is followed, first in the “infinite” geometry previously described and then in a realistic pixel geometry. The physics list includes both the previously mentioned processes and a modified version of the G4EmStandardPhysics_option4 physics list. This new version uses the G4ScreenedNuclearRecoil class to simulate the nuclear stopping of recoil atoms and explicitly generate all recoils [21, 22]. This class includes an energy cutoff for the production of recoil atoms. Except when explicitly mentioned, this cutoff is set at 100 eV/nucleon, i.e.

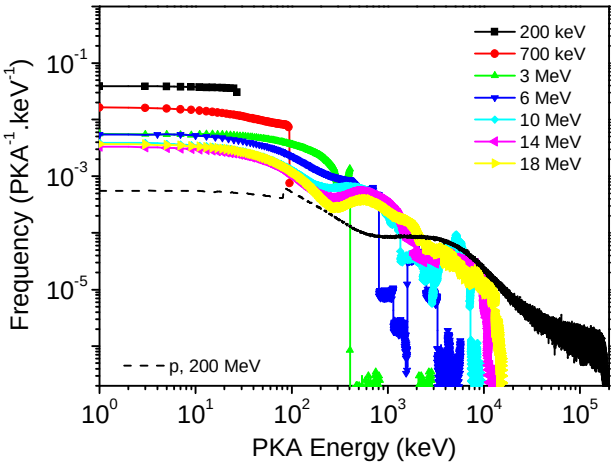

Figure 2: PKA energy spectra for different energies of incident neutrons and for 200 MeV protons in an infinite box of silicon.

~2.8 keV for silicon PKA, larger than the 1 keV limit of the BCA. The non-ionizing deposited energy is recorded for each incident particle. In the last case, the geometry is an array of 10x10x307 μm^3 silicon boxes topped by 10 µm SiO_2 overlayers, each box being representative of a single image sensor pixel. The incident particles are emitted randomly towards the top of the geometry; the "beam" size matches the box lateral dimensions. The non-ionizing deposited energy is only recorded in the 7 µm-thick epitaxial layer of the simulated pixel.

IV. Choice of "relevant" PKA

The first parameter extracted from simulations is the energy of the produced recoil atoms, or PKA, for different energies of incident neutrons (in the energy range of available experimental data). The resulting spectra are reported in Figure 2 for the infinite box of silicon, along with results for 200 MeV protons, to compare with the hundreds of MeV energy range for which experimental data also exist (above 50 MeV, neutrons and protons are expected to have similar effects). All results are normalized to the total number of PKA registered in the simulation.

From these first results, we see that the PKA energy spectra are quite different depending on the energy of incident neutrons. The main difference is in the maximum energies of PKA, spanning from hundreds of keV for 3 MeV neutrons to several MeV for 18 MeV neutrons. For 200 MeV incident protons, the maximum PKA energy goes above 100 MeV. The shape of the curve at 200 and 700 keV, almost completely flat, slightly differs from other energies which all present a flat portion followed by a decreasing one. Despite this difference consistent with experimental observations for low energy neutrons, the direct analysis of these PKA energy distributions is not sufficient to explain the experimentally observed independence of dark current on the particle energy and type.

These distributions are then further split into different groups depending on their atomic number Z: "low-Z" PKA and "high-Z" PKA. Indeed, the PKA species regroup a

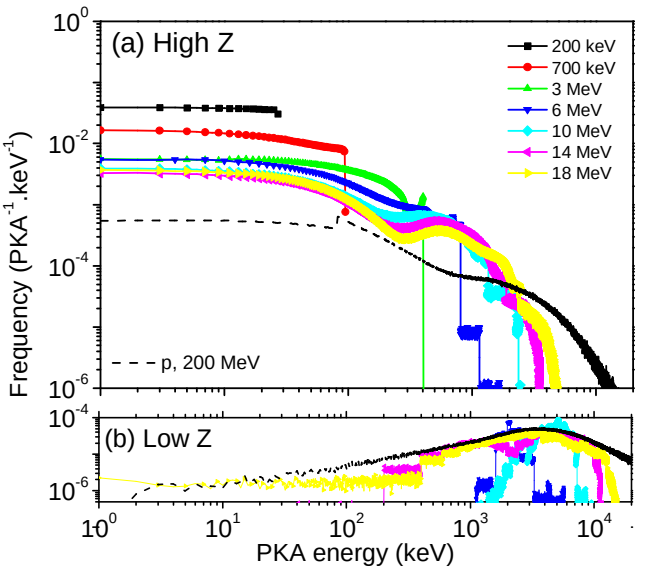

Figure 3: PKA energy spectra for different energies of incident neutrons and for 200 MeV protons: (a) high-Z PKA (8 to 15) and (b) low-Z PKA (1 or 7).

majority of silicon atoms, produced by elastic interactions, and recoil atoms produced by inelastic interactions (for incident neutrons, only above 3 MeV). In this last case, for each interaction, we find a "low-Z" PKA, with Z from 1 to 7 (limited to 1 and 2 for the neutron energies considered here) and "high-Z" PKA with Z from 8 to 15 (limited to Z of 12, 13 and 14 for neutrons here). The "high-Z" and "low-Z" PKA spectra are represented in Figures 3(a) and (b) respectively, showing that low-Z PKA correspond to the high energy part of the spectra. These light recoils will have much longer ranges than heavier particles (25 µm in silicon for a 5 MeV alpha for example, vs. 3 µm for a 5 MeV silicon recoil), are much less numerous, and deposit less than 10 keV of non-ionizing energy on their total range. They are thus not expected to be key contributors to DD in microvolumes of silicon and are ignored in the following.

Among "high-Z" PKA, for incident neutrons from 200 keV to 18 MeV, 100 to 67% are silicon ions; the proportion is 45% for 200 MeV protons. MD simulations in [18] will thus focus on this species. From Figure 3(a), these PKA energies go from 0 up to several MeV, with a clear decrease above 1 MeV, and a rather flat distribution up to 100 keV. The idea in the following is to see if large energy PKA cascades can be split up in subcascades generated by lower energy Secondary Knock-On Atoms (SKA), that would be easier to simulate in MD while being still representative of most recurrent defect configurations. To do so, PKA simulations are performed, to explore the energy distribution of second generation recoils (SKA in the following). For this step, the Geant4 recoil cutoff is set at its minimum value of 1 eV/nucleon, i.e. ~28 eV for silicon PKA, to be as close as possible to the 21 eV displacement threshold energy usually considered for silicon. The SKA energy spectra obtained for silicon PKA of 10 keV, 100 keV and 1 MeV in silicon are reported in Figure 4. They

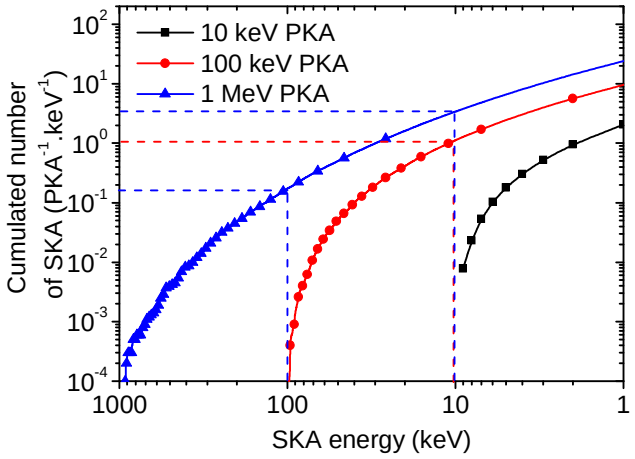

Figure 4: SKA energy spectra for different energies of silicon PKA.

TABLE I: AVERAGE NUMBER OF SKA WITH ENERGY LARGER THAN 28 EV, 1 KEV, 10 KEV AND 100 KEV FOR DIFFERENT PKA ENERGY.

Average number of SKA with energy...	PKA energy				
	1 keV	10 keV	100 keV	1 MeV	10 MeV
> 28 eV	5.1 *(5.1)*	16 *(13)*	56	163	283
> 1 keV	-	2	9.5	24	34
> 10 keV	-	-	1.1	3.4	4.7
> 100 keV	-	-	-	0.2	0.3

are represented as an average cumulated number of SKA per incident PKA depending on the SKA energy; the abscissa axis is reversed. Each point thus corresponds to the number of SKA with a larger energy than the abscissa, i.e. for 1 MeV PKA, 0.2 SKA have an energy larger than 100 keV and 3.4 SKA have an energy larger than 10 keV. Some values are also reported in Table I for easier reading and interpretation. The first line of the table for SKA with energy larger than 28 eV actually corresponds to the average total number of SKA generated in the simulation. Because of the limits of the BCA mentioned earlier, these values are considered as only indicative. For comparison, the values obtained with MD simulations in [18] for 1 and 10 keV PKA are reported in parenthesis. Both simulations are in good agreement for this parameter.

From this figure and table, most part of the distribution generated by 1 MeV or even 10 MeV PKA is below 100 keV. For each 1 MeV PKA, 3.4 SKA have an energy larger than 10 keV with only one larger than 30 keV. For each 100 keV PKA, 1.1 SKA have an energy larger than 10 keV. These large energy PKA cascades thus seem well represented by 10 keV subscascades. Moreover, these 10 keV SKA are randomly generated along the path of the larger energy PKA, which is on average of 1.1 and 4.8 µm respectively for 1 and 10 MeV silicon atoms in silicon. By comparison, the range of 10 keV silicon atoms is around 20 nm in silicon (the ranges are extracted from Geant4 and confirmed by SRIM simulations [23]). The 10 keV subcascades are thus not expected to overlap.

Similarly, 10 keV cascades could be represented by 1 keV

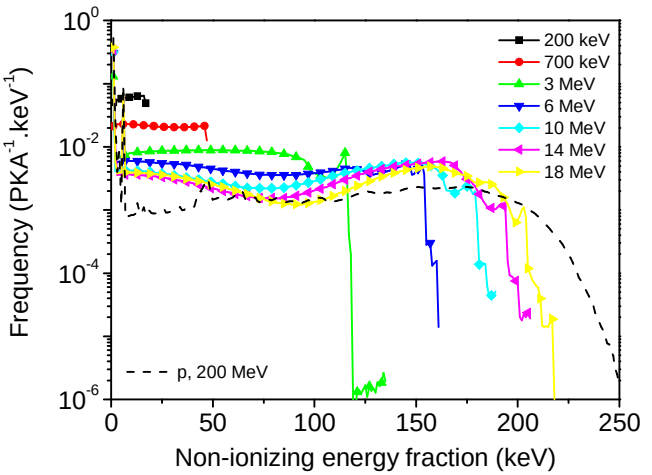

Figure 5: Fraction of the PKA energy spectra lost in non-ionizing events, for different energies of incident neutrons and for 200 MeV protons.

subcascades, but the risk of overlapping subcascades is then much more probable given the limited range of the 10 keV PKA. This could result in clusters larger than the ones directly generated by 1 keV PKA. 1 to 10 keV subcascades are however important contributors to the damage generated at all energies. For 1 keV, 4 out of 5 SKA are actually below 200 eV. They are expected to generate mostly point defects, or very small clusters. These findings are consistent with the partitioning of the PKA energy into free defects (PKA < 1-2 keV), one single cascade (between 1-2 and 12-20 keV) and multiple cascades (> 12-20 keV) proposed in [24].

From all these elements regarding the PKA characteristics, MD simulations presented in [18] thus focus on simulating the trajectory of 1 and 10 keV silicon atoms in silicon. The characteristics of resulting displacement cascades are analyzed, studying in particular the size of generated clusters. Some 100 keV cascade simulations are also shown, for comparison with 10 keV, to assess the pertinence of focusing on this lower energy.

V. NON-IONIZING DEPOSITED ENERGY DISTRIBUTION

To go further in the analysis of MC simulations, the second parameter extracted from simulations is the energy actually going into DD for the previously calculated distributions of PKA. Two different kinds of calculations are actually performed here: the total non-ionizing energy **lost** by the PKA in an infinite geometry, and the non-ionizing energy **deposited** in microvolumes of silicon of different dimensions.

A. Infinite geometry

At first, the energy portion going into non-ionizing events is simply calculated from the PKA spectrum extracted in the first type of simulation, using the Lindhard-Robinson partition factor [25, 26]. The module G4LindhardPartition developed by M. Mendenhall [22] following the formulation from [27] is used for this calculation. This factor allows a simple theoretical calculation giving the fraction of the total kinetic energy of an ion going into electronic stopping and the fraction

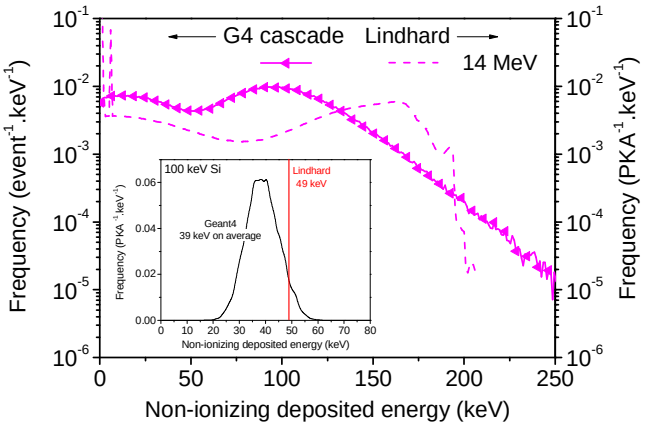

Figure 6: Non-ionizing deposited energy events obtained from full cascade Geant4 simulation, compared with theoretical non-ionizing energy fraction from the Lindhard partition for 14 MeV neutrons in an infinite geometry. The inset shows the non-ionizing deposited energy distribution for a 100 keV silicon atom obtained with Geant4, compared with the single value given by the Lindhard partition.

TABLE II: NON-IONIZING ENERGY LOSS FROM LINDHARD THEORETICAL CALCULATIONS AND NON-IONIZING ENERGY DEPOSIT FROM FULL CASCADE SIMULATIONS WITH GEANT4 AND SRIM, FOR DIFFERENT PKA ENERGY.

PKA energy	Non-ionizing energy loss (Lindhard) [keV]	Non-ionizing energy deposit (full cascade) – [keV]	
		Geant4	SRIM
10 keV	6.9	6.3	5.8
100 keV	49	39	37
1 MeV	164	118	120
10 MeV	240	176	176

going into DD, on the total range of the ion.

The result of applying this partition factor to the PKA spectrum from Figure 2 is reported in Figure 5. From this figure, it appears that the distributions of non-ionizing lost energy are very similar for all neutron energies, with an almost "flat" distribution, only going to larger values for higher incident neutron energy. However, this difference in maximum energy remains much more limited (~one order of magnitude), compared to the differences observed in the PKA energy spectrum in Figure 2 (~three orders of magnitude). 200 MeV proton results are also reported, showing a distribution remarkably similar to neutron ones, with again a maximum energy not so much larger than for incident neutrons of much lower energy. For energies larger than 3 MeV, the difference is even reduced to a factor 2, from ~125 keV for 3 MeV neutrons to ~250 keV for 200 MeV protons. The discrepancy with low energy neutrons is again more pronounced, with a maximum of ~20 and 50 keV only for 200 and 700 keV neutrons respectively. These results provide a first justification for the similarities found in measured electrical effects in image sensors, with empirical models working for different particles on large energy ranges, with slight differences for low energy neutrons.

Before simulating a realistic geometry, an intermediate step is performed, explicitly following the PKA trajectory and its generated cascade in the infinite geometry, and recording the resulting non-ionizing deposited energy. The result is reported in Figure 6 for 14 MeV neutrons, in comparison with the use of the Lindhard partition presented in Figure 5. While the values of non-ionizing deposited energy are consistent, the shape of the curves slightly differs. This discrepancy first comes from the difference between a theoretical model giving a fixed average value of non-ionizing energy loss and the actual simulation of the cascade, with dispersion in this non-ionizing energy loss for a given energy, as illustrated in the inset of Figure 6 for a 100 keV silicon atom in silicon. Moreover, the average value of non-ionizing energy deposit obtained with Geant4 is slightly lower than the one obtained from the Lindhard partition. The values are reported in Table II for different silicon PKA energies, comparing the value of non-ionizing energy loss obtained with the Lindhard partition, with a full cascade simulation in Geant4 and SRIM. The difference between Lindhard and Geant4 is expected from [21]. Geant4 values are however on the same order of magnitude as Lindhard, and in good agreement with the values obtained from SRIM in full damage cascade mode.

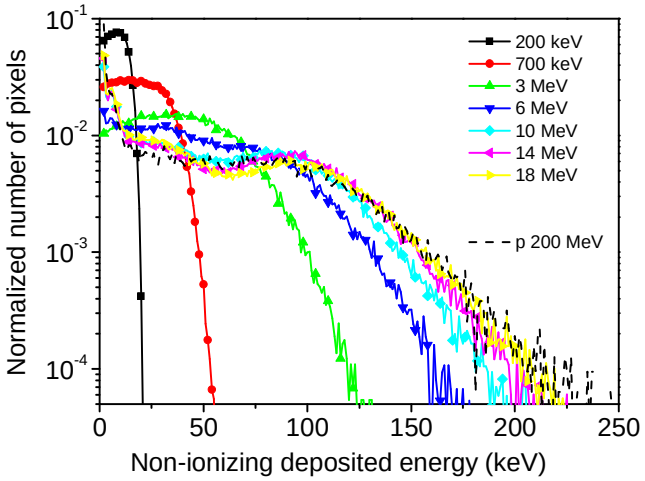

Figure 7: Non-ionizing deposited energy events recorded in an array of pixels, for different energies of incident neutrons.

So, while the resulting absolute values of energy deposit must be considered cautiously, Geant4 full cascade simulations are considered as qualitatively correct. The change in shape in Figure 6 shows the limits of using only an analytical formula such as the Lindhard partition to estimate the non-ionizing deposited energy distribution. In the following, the effect of a finite geometry on this shape is further explored.

B. Finite size geometry

In a final simulation step, a simulation box closer to an image sensor geometry is simulated and all secondary trajectories are followed. The resulting non-ionizing energy deposits are registered in an array of 10x10 μm^2 pixels. The result is reported in Figure 7 for different neutron energies and 200 MeV protons. The distributions are normalized to the number of pixels recording an event. This means that for one incident neutron, several events can be counted, in case of border crossing effects (i.e. DD cascades extending over

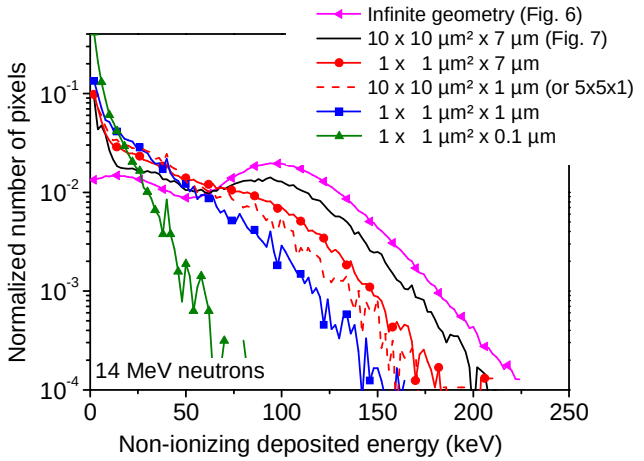

Figure 8: Influence of the pixel geometry (surface x depth) on the distribution, for 14 MeV incident neutrons.

several pixels, or extending deeper than the pixel depth and partially going out of the depletion region).

Again, the shape of the curves slightly differs from the ones presented in Figure 6, corresponding to a geometrical effect. However, the similarities between all distributions remain. The data for energies larger than 6 MeV are almost superimposed, while 200 keV and 700 keV distributions clearly differ. The 3 MeV neutron curve appear like a transition regime, tending towards the higher energy tendency. This provides again first hints for the similarities observed in experimental data for all these energies up to 200 MeV, with a different behavior for lower energy neutrons.

Finally, the effect of the pixel size on the non-ionizing deposited energy distributions is further explored, to see when (if) border crossing effects start to change the distribution shape. Results are shown in Figure 8, for different pixel geometries, for 14 MeV incident neutrons. The results from Figure 6 in an infinite geometry are also reported for reference. The shape of this curve is very similar to the shape obtained in Figure 7 for 10x10 µm² x 7 µm pixels. Two parameters are explored: the pixel width and depth, first changed separately and then together. Reducing the width of the pixels to 1 µm without changing the depth (1 µm² x 7 µm, solid red curve with circles) slightly changes the shape. Reducing the depth of the pixels to 1 µm without changing the width (10x10 µm² x 1 µm, dotted red curve) has more impact on the distribution shape, and is more likely to correspond to realistic cases (1 µm is a typical order of magnitude of depletion depth in CIS). Moreover, with this small depth of 1 µm, reducing the width to 5 µm has no further impact. Such 5x5x1 μm^3 volume well corresponds to the smallest pixels generally used in radiation environment. The 1 μm^3 pixel case is also reported, shifting again the curve to the left. This last case is more representative of state of the art pixel size used for mass market applications (smartphones for example), but generally not exposed to radiation fields. Further reducing the depth of pixels to 0.1 µm (green curve) emphasizes the general trend, but is not actually representative of current technology. From these results, only for technologies having pixel depth approaching 1 µm, will the general shape of the distribution start to change significantly. This is consistent with experimental results on the smallest pinned photodiode CMOS image sensors [28], for which the [8] empirical model parameters had to be changed to keep working. This change remains rather limited for larger pixels, thus indicating that the general empirical models developed for example in [8] should keep working for the pixel sizes usually used in space application and other scientific application in radiation environments.

VI. Conclusion

MC simulations of different energy neutrons and protons incident on silicon are performed, looking at different parameters characterizing the particle-matter interactions. The analysis demonstrates that while PKA energy spectra greatly depend on the incident particle energy and species, in particular in terms of maximum energy, distributions of non-ionizing energy loss/deposit are remarkably similar. This result provides, for the first time to our knowledge, first elements that could justify the resulting similar electrical effects measured on image sensors for different incident radiations.

However, these results are not sufficient to actually fully understand the mechanisms at stake at the atomic level and make direct link with experimental data. That is why, the MC simulations presented in this study are also part of a larger simulation project gathering different methods following the approach presented by Srour and Palko in their NSREC 2013 Short Course [15]. In this original approach, the results obtained here will guide the choice of input for the next level of simulation, i.e. MD simulation, by identifying relevant PKA. The MD simulation detailed in the second part of this study [18] will thus be focused on the study of silicon recoils in the 1-10 keV energy range, incident in silicon, identified as the representative contributors to displacement damage in this paper. The following steps of the simulation approach, generating the full displacement cascade and following its evolution up to the second timescale will allow identifying the defects responsible for experimental measurements through the characterization of their electronic properties. Only through this complete simulation process can these effects be understood, in the hope that in the end, mitigating techniques can be deduced from their analysis.

Acknowledgement

The authors would like to thank J. Srour for helpful communications.

References

[1] J. R. Srour, S. C. Chen, S. Othmer, and R. A. Hartmann, "Radiation damage coefficients for silicon depletion regions," *IEEE Trans. Nucl. Sci.*, vol. 26, pp. 4784 - 4791, 1979.

[2] C. J. Dale, P. W. Marshall, E. A. Burke, G. P. Summers, and G. E. Bender, "The generation lifetime damage factor and its variance in silicon," *IEEE Trans. Nucl. Sci.*, vol. 36, pp. 1872 - 1881, 1989.

[3] J. R. Srour and D. H. Lo, "Universal damage factor for radiation-induced dark current in silicon devices," *IEEE Trans. Nucl. Sci.*, vol. 47, pp. 2451 - 2459, 2000.

[4] P. W. Marshall, C. J. Dale, E. A. Burke, G. P. Summers, and G. E. Bender, "Displacement damage extremes in silicon depletion regions," *IEEE Trans. Nucl. Sci.*, vol. 36, pp. 1831 - 1839, 1989.

[5] C. J. Dale, P. W. Marshall, and E. A. Burke, "Particle-induced spatial dark current fluctuations in focal plane arrays," *IEEE Trans. Nucl. Sci.*, vol. 37, pp. 1784 - 1791, 1990.

[6] P. W. Marshall, C. J. Dale, and E. A. Burke, "Proton-induced displacement damage distributions and extremes in silicon microvolumes," *IEEE Trans. Nucl. Sci.*, vol. 37, pp. 1776 - 1783, 1990.

[7] C. J. Dale, L. Chen, P. J. McNulty, P. W. Marshall, and E. A. Burke, "A comparison of Monte Carlo and analytic treatments of displacement damage in Si microvolumes," *IEEE Trans. Nucl. Sci.*, vol. 41, pp. 1974 - 1983, 1994.

[8] C. Virmontois, V. Goiffon, P. Magnan, S. Girard, O. Saint-Pé, S. Petit, G. Rolland, and A. Bardoux, "Similarities between proton and neutron induced dark current distribution in CMOS image sensors," *IEEE Trans. Nucl. Sci.*, vol. 59, pp. 927 - 236, 2012.

[9] M. Raine, V. Goiffon, P. Paillet, O. Duhamel, S. Girard, M. Gaillardin, C. Virmontois, J.-M. Belloir, N. Richard, and P. Magnan, "Exploring the kinetics of formation and annealing of single particle displacement damage in microvolumes of silicon," *IEEE Trans. Nucl. Sci.*, vol. 61, pp. 2826 - 2833, 2014.

[10] J.-M. Belloir, V. Goiffon, C. Virmontois, M. Raine, P. Paillet, O. Duhamel, M. Gaillardin, R. Molina, P. Magnan, and O. Gilard, "Pixel pitch and particle energy influence on the dark current distribution of neutron irradiated CMOS image sensors," *Optics Express*, vol. 24, pp. 4299 - 4315, 2016.

[11] J. R. Srour and J. W. Palko, "A framework for understanding displacement damage mechanisms in irradiated silicon devices," *IEEE Trans. Nucl. Sci.*, vol. 53, pp. 3610 - 3620, 2006.

[12] C. Inguimbert, T. Nuns, M. C. Ursule, D. Falguere, D. Herve, M. Beaumel, and M. Poizat, "Modeling the dark current non-uniformity of image sensors with Geant4," *IEEE Trans. Nucl. Sci.*, vol. 61, pp. 3323 - 3330, 2014.

[13] M. T. Robinson and I. M. Torrens, "Computer simulation of atomic displacement cascades in solids in the binary-collision approximation," *Phys. Rev. B*, vol. 9, pp. 5008 - 5024, 1974.

[14] G. P. Mueller and C. S. Guenzer, "Simulations of cascade damage in silicon," *IEEE Trans. Nucl. Sci.*, vol. 27, pp. 1474 - 1477, 1980.

[15] J. R. Srour and J. W. Palko, "Displacement damage effects in devices," Short Course of the Nuclear and Space Radiation Effects Conference (NSREC), San Francisco, 2013.

[16] G. Hobler and G. Betz, "On the useful range of application of molecular dynamics simulations in the recoil interaction approximation," *Nucl. Instr. and Meth. in Phys. Res. B*, vol. 180, pp. 203 - 208, 2001.

[17] L. K. Beland and N. Mousseau, "Long-time relaxation of ion-bombarded silicon studied with the kinetic activation-relaxation technique: Microscopic description of slow aging in a disordered system," *Phys. Rev. B*, vol. 88, pp. 214201, 2013.

[18] A. Jay, M. Raine, N. Mousseau, N. Richard, V. Goiffon, A. Hemerick, and P. Magnan, "Simulation of Single Particle Displacement Damage in Silicon – Part II: Generation and Long Time Relaxation of the Damage Structure," *IEEE Trans. Nucl. Sci.*, vol. 64, 2016.

[19] S. Agostinelli, J. Allison, K. Amako, J. Apostolakis, H. Araujo, P. Arce, M. Asai, D. Axen, S. Banerjee, G. Barrand, F. Behner, L. Bellagamba, J. Boudreau, L. Broglia, A. Brunengo, H. Burkhardt, S. Chauvie, J. Chuma, R. Chytracek, G. Cooperman, G. Cosmo, P. Degtyarenko, A. Dell'Acqua, G. Depaola, D. Dietrich, R. Enami, A. Feliciello, C. Ferguson, H. Fesefeldt, G. Folger, F. Foppiano, A. Forti, S. Garelli, S. Giani, R. Giannitrapani, D. Gibin, J. J. Gómez Cadenas, I. González, G. Gracia Abril, G. Greeniaus, W. Greiner, V. Grichine, A. Grossheim, S. Guatelli, P. Gumplinger, R. Hamatsu, K. Hashimoto, H. Hasui, A. Heikkinen, A. Howard, V. Ivanchenko, A. Johnson, F. W. Jones, J. Kallenbach, N. Kanaya, M. Kawabata, Y. Kawabata, M. Kawaguti, S. Kelner, P. Kent, A. Kimura, T. Kodama, R. Kokoulin, M. Kossov, H. Kurashige, E. Lamanna, T. Lampén, V. Lara, V. Lefebure, F. Lei, M. Liendl, W. Lockman, F. Longo, S. Magni, M. Maire, E. Medernach, K. Minamimoto, P. Mora de Freitas, Y. Morita, K. Murakami, M. Nagamatu, R. Nartallo, P. Nieminen, T. Nishimura, K. Ohtsubo, M. Okamura, S. O'Neale, Y. Oohata, K. Paech, J. Perl, A. Pfeiffer, M. G. Pia, F. Ranjard, A. Rybin, S. Sadilov, E. Di Salvo, G. Santin, T. Sasaki, N. Savvas, Y. Sawada, et al., "GEANT4 - A simulation toolkit," *Nucl. Instr. and Meth. in Phys. Res. A*, vol. 506, pp. 250 - 303, 2003.

[20] J. Allison, K. Amako, J. Apostolakis, H. Araujo, P. Arce Dubois, M. Asai, G. Barrand, R. Capra, S. Chauvie, R. Chytracek, G. A. P. Cirrone, G. Cooperman, G. Cosmo, G. Cuttone, G. G. Daquino, M. Donszelmann, M. Dressel, G. Folger, F. Foppiano, J. Generowicz, V. Grichine, S. Guatelli, P. Gumplinger, A. Heikkinen, I. Hrivnacova, A. Howard, S. Incerti, V. Ivanchenko, T. Johnson, F. Jones, T. Koi, R. Kokoulin, M. Kossov, H. Kurashige, V. Lara, S. Larsson, F. Lei, O. Link, F. Longo, M. Maire, A. Mantero, B. Mascialino, I. McLaren, P. Mendez Lorenzo, K. M. K. Minamimoto, P. Nieminen, L. Pandola, S. Parlati, L. Peralta, J. Perl, A. Pfeiffer, M. G. Pia, A. Ribon, G. R. P. Rodrigues, S. Sadilov, G. Santin, T. Sasaki, D. Smith, N. Starkov, S. Tanaka, E. Tcherniaev, B. Tomé, and P. T. A. Trindade, L. Urban, M. Verderi, A.Walkden, J. P.Wellisch, D. C.Williams, D. Wright, and H. Yoshida, "Geant4 developments and applications," *IEEE Trans. Nucl. Sci.*, vol. 53, pp. 270 - 278, 2006.

[21] R. A. Weller, M. H. Mendenhall, and D. M. Fleetwood, "A screened coulomb scattering module for displacement damage computations in Geant4," *IEEE Trans. Nucl. Sci.*, vol. 51, pp. 3669 - 3678, 2004.

[22] M. H. Mendenhall and R. A. Weller, "An algorithm for computing screened Coulomb scattering in GEANT4," *Nucl. Instr. and Meth. in Phys. Res. B*, vol. 227, pp. 420 - 430, 2005.

[23] "SRIM," pp. http://www.srim.org.

[24] S. Wood, N. J. Doyle, J. A. Spitznagel, W. J. Choyke, R. M. More, J. N. McGruer, and R. B. Irwin, "Simulation of radiation damage in solids," *IEEE Trans. Nucl. Sci.*, vol. 28, pp. 4107 - 4112, 1981.

[25] J. Lindhard, V. Nielsen, M. Scharff, and P. V. Thomsen, "Integral equations governing radiation effects (Notes on atomic collisions, III)," *Mat. Fys. Medd. Dan. Vid. Selsk.*, vol. 33, pp. 1 - 42, 1963.

[26] M. T. Robinson, "The dependence of radiation effects on primary recoil energy," *Proc. Int. Conf. Radiation-Induced Voids in Metals*, pp. 397 - 429, 1972.

[27] I. Jun, "Effects of secondary particles on the total dose and the displacement damage in space proton environments," *IEEE Trans. Nucl. Sci.*, vol. 48, pp. 162 - 175, 2001.

[28] C. Virmontois, V. Goiffon, F. Corbiere, P. Magnan, S. Girard, and A. Bardoux, "Displacement damage effects in pinned photodiode CMOS image sensors," *IEEE Trans. Nucl. Sci.*, vol. 59, pp. 2872 - 2877, 2012.